

DISCOVERY OF EXTENDED MAIN SEQUENCE TURN-OFFS IN FOUR YOUNG MASSIVE CLUSTERS IN THE MAGELLANIC CLOUDS

CHENGYUAN LI

Department of Physics and Astronomy, Macquarie University, Sydney, NSW 2109, Australia

RICHARD DE GRIJS

Kavli Institute for Astronomy & Astrophysics and Department of Astronomy, Peking University, Yi He Yuan Lu 5, Hai Dian District, Beijing 100871, China
and

International Space Science Institute–Beijing, 1 Nanertiao, Zhongguancun, Hai Dian District, Beijing 100190, China

LICAI DENG

Key Laboratory for Optical Astronomy, National Astronomical Observatories, Chinese Academy of Sciences, 20A Datun Road, Chaoyang District, Beijing 100012, China

ANTONINO P. MILONE

Research School of Astronomy & Astrophysics, Australian National University, Mt Stromlo Observatory, Cotter Road, Weston, ACT 2611, Australia

ABSTRACT

An increasing number of young massive clusters (YMCs) in the Magellanic Clouds have been found to exhibit bimodal or extended main sequences (MSs) in their color–magnitude diagrams (CMDs). These features are usually interpreted in terms of a coeval stellar population with different stellar rotational rates, where the blue and red MS stars are populated by non- (or slowly) and rapidly rotating stellar populations, respectively. However, some studies have shown that an age spread of several million years is required to reproduce the observed wide turn-off regions in some YMCs. Here we present the ultraviolet–visual CMDs of four Large and Small Magellanic Cloud YMCs, NGC 330, NGC 1805, NGC 1818, and NGC 2164, based on high-precision Hubble Space Telescope photometry. We show that they all exhibit extended main-sequence turn-offs (MSTOs). The importance of age spreads and stellar rotation in reproducing the observations is investigated. The observed extended MSTOs cannot be explained by stellar rotation alone. Adopting an age spread of 35–50 Myr can alleviate this difficulty. We conclude that stars in these clusters are characterized by ranges in both their ages and rotation properties, but the origin of the age spread in these clusters remains unknown.

Keywords: globular clusters: individual: NGC 330, NGC 1805, NGC 1818, NGC 2164 — Hertzsprung–Russell and C–M diagrams — Magellanic Clouds

1. INTRODUCTION

The origin of the multiple stellar populations that have been discovered in almost all Galactic globular clusters (GCs) remains an open question (Gratton et al. 2004; Piotto et al. 2015). Since it is not possible to observe the young GCs in the early Universe, studying young GC candidates in the Milky Way and its satellites therefore plays a fundamental role in addressing this issue. However, almost all young Galactic clusters are located in the Galactic disk. They are affected by severe foreground extinction, which may mask the multiple stellar populations in their observed color–magnitude diagrams (CMDs).

An alternative way is to study the young clusters in the Large and Small Magellanic Clouds (LMC and SMC). Current observations of star clusters in the LMC and SMC mainly reveal two features: (a) almost all intermediate-age

(1–2 Gyr-old) star clusters exhibit extended main sequence turn-offs (eMSTOs; e.g., Bertelli et al. 2003; Mackey & Broby Nielsen 2007; Milone et al. 2009; Girardi et al. 2013; Li et al. 2014a), while some even exhibit extended or dual red clumps (Girardi et al. 2009; Li et al. 2016a); (b) some young massive clusters (YMCs; with ages ≤ 400 Myr) in the LMC exhibit bimodal or extended main sequences (MSs) (Milone et al. 2015; Bastian et al. 2016; Milone et al. 2016, 2017).

The discovery of eMSTO regions in intermediate-age clusters has triggered a surge of interest in explaining this feature, starting from the age-spread scenario, which attributes the observed eMSTOs to primordial age spreads of up to 700 Myr (Goudfrooij et al. 2011; Girardi et al. 2013; Goudfrooij et al. 2014; Girardi 2016). Next came the rapid stellar rotation scenario (Bastian & de Mink 2009; Yang et al. 2013; Li et al. 2014b; Brandt & Huang 2015; Bastian & Niederhofer 2015; Li et al. 2016a; Wu et al. 2016). Recently, a new scenario has been suggested, i.e., that stellar variability may play a potential role in shaping the eMSTO regions as well (Salinas et al. 2016; de Grijs 2017). The debate is indeed heating up.

Further excitement was added by the discovery of bimodal or extended MSTOs in YMCs. These features are usually explained by a coeval stellar population with a dispersion in stellar rotation rates (Li et al. 2014a,b; Bastian et al. 2016) or a coeval, rapidly rotating population combined with a slowly/non-rotating population exhibiting an age spread (Milone et al. 2017). It has been suggested that the blue MS stars may hide a binary component, where binary synchronization is responsible for their small rotational rates (D’Antona et al. 2015). A recent study based on the YMCs NGC 1866 and NGC 1850 showed that a coeval stellar population featuring a distribution of stellar rotation rates can only partially explain the broadening of the MSTO (Milone et al. 2017; Correnti et al. 2017).

In this paper, we study four YMCs in the LMC and SMC, i.e., NGC 330 (SMC), NGC 1805, NGC 1818, and NGC 2164. Their isochronal ages do not exceed 40 Myr, 40 Myr, 35 Myr, and 100 Myr, respectively. Most are younger than the recently studied YMCs (e.g., Li et al. 2017; Milone et al. 2015, 2016, 2017). We analyzed their CMDs using high-resolution *Hubble Space Telescope* (*HST*) photometry, obtained using ultraviolet and visual filters. We find that they all exhibit extended MSTOs, although at different levels of significance. We test whether the observations can be reproduced assuming an age spread, a dispersion in stellar rotation rates, or a combination of these scenarios.

This article is arranged as follows. Section 2 presents our data reduction, which is followed by the main results of our analysis in Section 3. In Section 4 we present a discussion. Section 5 summarizes and concludes the paper.

2. DATA REDUCTION

The data used in this work come from the *HST* Ultraviolet and Visual Channel of the Wide Field Channel 3 (UVIS/WFC3) and Wide Field and Planetary Camera 2 (WFPC2) images. The WFC3/UVIS images were observed through the F225W and F336W passbands and the *HST*/WFP2 images were observed in the F555W and F814W bands. Relevant information pertaining to the data is summarized in Table 1.

Table 1. Inventory of the data set used in this work

Cluster	Camera	exposure time	filter	program ID	PI name
NGC 330	WFC3/UVIS	10 s + 100 s + 805 s + 3×960 s	F336W	GO-13727	J. Kalirai
	WFPC2	10 s + 4×350 s	F555W	GO-8134	A. Nota
NGC 1805	WFC3/UVIS	10 s + 100 s + 790 s + 3×947 s	F336W	GO-13727	J. Kalirai
	WFPC2	3×5 s + 3×140 s + 2×800 s + 900 s	F555W	GO-7307	G. Gilmore
NGC 1818	WFC3/UVIS	10 s + 100 s + 790 s + 3×947 s	F336W	GO-13727	J. Kalirai
	WFPC2	3×5 s + 3×140 s + 2×800 s + 900 s	F555W	GO-7307	G. Gilmore
NGC 2164	WFC3/UVIS	10 s + 100 s + 790 s + 3×947 s	F336W	GO-13727	J. Kalirai
	WFPC2	10 s + 4×350 s	F555W	GO-8134	A. Nota

As regards the WFC3/UVIS and WFPC2 images, we performed point-spread-function (PSF) photometry on the ‘_flt’ or ‘_c0m’ frames using the WFC3 and WFPC2 module of the DOLPHOT 2.0 photometry package (Dolphin 2011a,b, 2013). To obtain a stellar catalog with high-quality photometry, we adopted a filter employing the sharpness and ‘crowding’ parameters calculated by DOLPHOT. The sharpness is a measure comparing the profile of an object relative

to the PSF. A perfect star would have a sharpness of zero. A negative sharpness that is too small usually indicates a cosmic ray, while a very large positive sharpness means that the detected object is extended, probably a background galaxy. The crowding parameter quantifies how much brighter a star would have been measured had nearby stars not been fitted simultaneously (in units of magnitudes). For an isolated star, the crowding is zero. High crowding usually means that the star is poorly measured. We confirmed that most high-crowding objects are faint, which would not dramatically affect our analysis. We only selected objects with $-0.2 \leq \text{sharpness} \leq 0.2$ and $\text{crowding} \leq 0.5$ in both frames, which left us with $\sim 70\%$ of the objects with high-accuracy photometry. The number of objects before and after the selection (in brackets) for the clusters NGC 330, NGC 1805, NGC 1818, and NGC 2164 were 9996 (7208), 3808 (3102), 4478 (3346), and 4284 (3322), respectively. DOLPHOT can automatically flag ‘good stars’ and centrally saturated objects. We only kept objects that were indicated as good in our final sample for further analysis.

For each cluster, we combined stellar catalogs of different exposure times into a deep catalog. If one star appeared in two stellar catalogs, we selected the longest exposure time as best representation. Next, we obtained two stellar catalogs, derived from the WFC3/UVIS and WFPC2 images. We transferred each star’s CCD coordinates to equatorial coordinates ($X, Y \rightarrow \alpha_{J2000}, \delta_{J2000}$). We only selected stars located in the areas covered by both CCD fields for each cluster. This process sacrifices a large field but provides us with deep, multi-band stellar catalogs.

We used the method introduced by [Milone et al. \(2012, their Section 3.1\)](#) to calculate differential reddening maps. We corrected all stars for differential reddening by assuming $A_{\text{UVIS}, F336W} = 1.658 A_V$ and $A_{\text{WFPC2}, F555W} = 1.017 A_V$. We found that differential reddening does not dramatically change the morphology of our CMDs.

We generated number-density contour figures to determine the center coordinates of our clusters. We simply assigned the coordinate where the number density reaches the highest value as the cluster center. We then used the number-density center to define a circular region within twice the half-light radius ($2r_{\text{hl}}$) as the cluster region. The r_{hl} values were taken from [McLaughlin & van der Marel \(2005\)](#), which were based on fits to a Wilson model ([Wilson 1975](#))¹. In Fig. 1 we show the stellar spatial distributions, as well as their corresponding cluster centers and number-density contours. We confirmed that for all clusters, the stellar number density decreased to the field level at $2r_{\text{hl}}$. The clusters’ structural parameters are included in Table 2.

Table 2. Structural parameters

Cluster	α_{J2000}	δ_{J2000}	h_c (pc)	h_{hl} (pc)
			(1)	(2)
NGC 330	00 ^h 56 ^m 31.00 ^s	−72°27′55.80″	2.47 ^{+0.14} _{−0.19}	6.95 ^{+0.96} _{−0.43}
NGC 1805	05 ^h 02 ^m 22.14 ^s	−66°06′41.40″	1.34 ^{+0.09} _{−0.10}	2.86 ^{+0.13} _{−0.08}
NGC 1818	05 ^h 04 ^m 13.44 ^s	−66°26′02.40″	2.36 ^{+0.08} _{−0.09}	5.05 \pm 0.08
NGC 2164	05 ^h 58 ^m 55.80 ^s	−68°30′59.40″	1.69 ^{+0.09} _{−0.05}	4.37 ^{+0.05} _{−0.09}

NOTE— (1), (2): [McLaughlin & van der Marel \(2005\)](#)

The final step is field-star decontamination. For NGC 330, NGC 1805, NGC 1818, and NGC 2164, we adopt stars that are located beyond $3.75r_{\text{hl}}$, $6.00r_{\text{hl}}$, $4.00r_{\text{hl}}$, and $4.00r_{\text{hl}}$, respectively, as our reference field stars. This choice results in numbers of field stars close to ~ 500 for all clusters. We decontaminated the cluster CMDs using a similar method to that employed by [Li et al. \(2013a\)](#). We divided both the cluster and field CMDs into a carefully considered number of cells and counted the number of stars in each. The adopted numbers of grid cells were used to determine a reasonable average size for the grid cells. They should contain enough field stars to statistically correct the cluster CMDs, but they should not be too large, since that would prevent us from distinguishing detailed features along the MSs. Finally we randomly removed stars corresponding to those in the area-corrected field-star CMDs from the cluster CMDs. We found that our method tends to oversubtract field stars in the faint tail of the MS. This is because the field regions usually have lower detection limits than the clusters’ central regions because of crowding and background

¹ [Wilson \(1975\)](#) models are spherical and isotropic versions of models usually applied to elliptical galaxies. [McLaughlin & van der Marel \(2005\)](#) found that for $\sim 90\%$ of their full sample of YMCs and old GCs, [Wilson \(1975\)](#) models provide equally good or significantly better fits than [King \(1966\)](#) models

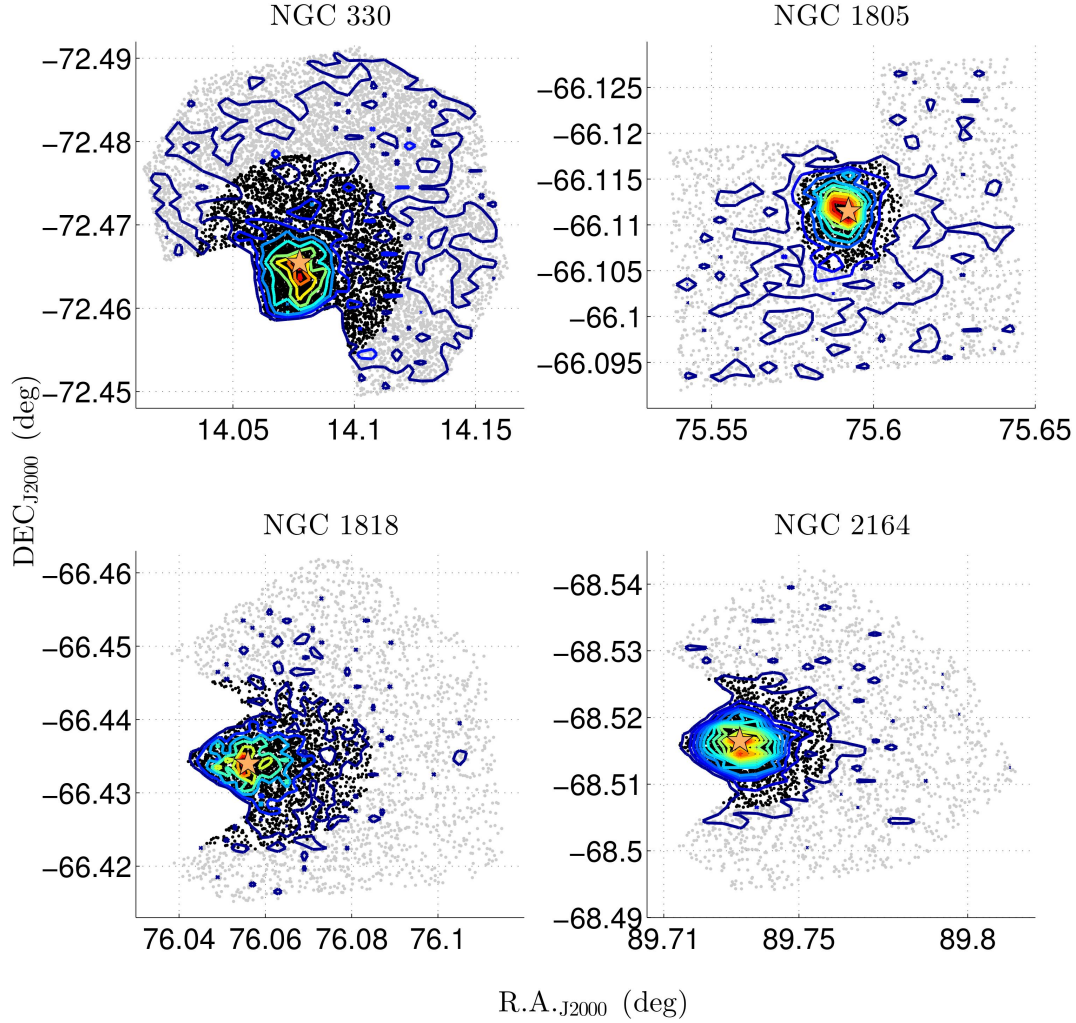


Figure 1. Spatial distributions of all stars (gray dots) and sample stars within two half-light radii (black dots). The cluster centers are indicated by orange pentagrams. The corresponding number-density contours are included. Since the field fluctuations are very small compared to the central density levels, for NGC 1818 and NGC 2164 there are no apparent density contours in the outer fields.

effects (which results in higher completeness levels for the field samples at the bottom of the MSs; see Fig. 7 of Li et al. 2013a). In this paper, we only focus on the MS range covering $F555W \leq 21$ mag, which is ~ 3 mag brighter than the magnitude of the detection limits. Our field-star contamination is thus reliable for the bright MSs.

3. MAIN RESULTS

The decontaminated YMC CMDs are presented in Fig. 2. Here we only present the (F555W versus F336W–F555W) CMDs, because the broadening of the MS is most obvious in this parameter space. Nevertheless, this feature can be detected in other ultraviolet–visual CMDs as well, e.g., in the (F814W versus F336W–F814W) CMDs. As shown in Fig. 2, all clusters exhibit wide MSs. We show the distribution of reference field stars in the same CMD. Because the clusters’ broadened MS regions are bright, contamination by field stars is minimal.

We next used different isochrones to fit the observations. Specifically, we used two different stellar evolution models to compare with the observations, i.e., the Geneva SYCLIST code (Ekström et al. 2012; Georgy et al. 2013, 2014)² and the MESA Isochrone & Stellar Tracks (MIST) models (Paxton et al. 2011, 2013, 2015; Dotter 2016; Choi et al. 2016)³. We first used the Geneva SYCLIST database to test if a coeval population of stars characterized by different

² <https://obswww.unige.ch/Recherche/evoldb/index/>

³ <http://waps.cfa.harvard.edu/MIST/>

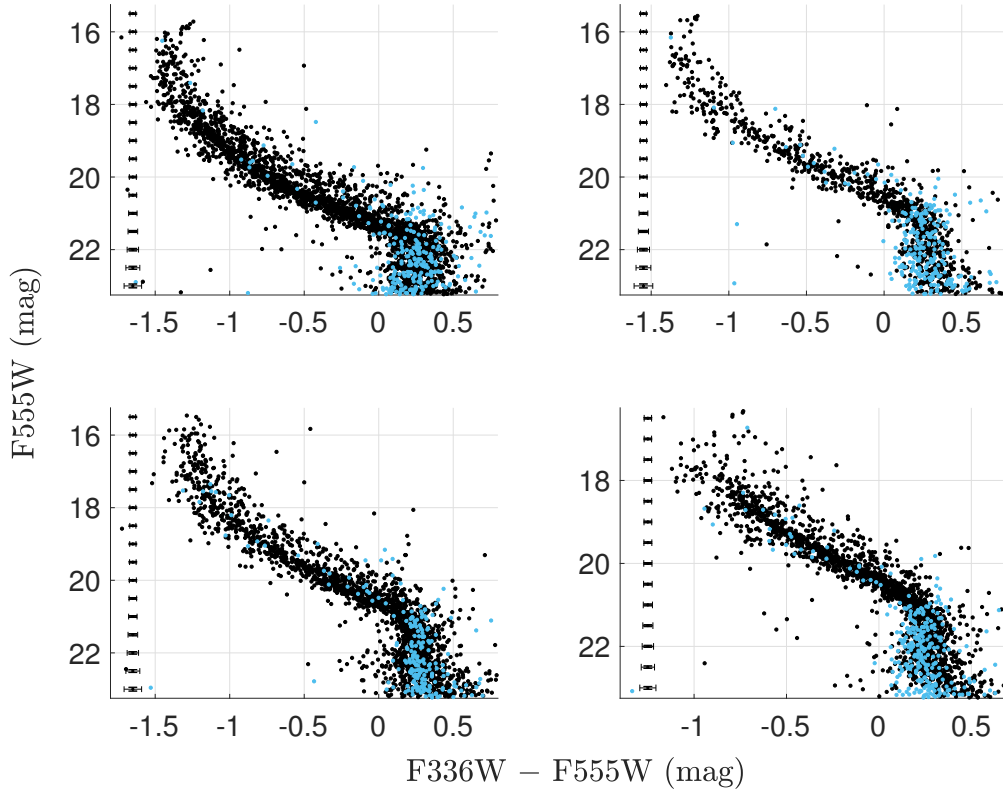


Figure 2. Decontaminated CMDs of NGC 330, NGC 1805, NGC 1818, and NGC 2164. The reference field stars (blue circles) are also shown. The corresponding average (1σ) photometric uncertainties are shown on the left-hand sides of all panels.

rotation rates could reproduce the observations. We overplotted nine Geneva isochrones with rotation rates of $\omega = 0.0$ – 0.95^4 to the observed CMD, where ω represent the ratio of the stellar rotation rate to the critical, breakup rate. All isochrones have the same age. The effects of extinction are not included in the Geneva models; we simply shifted the isochrones to match the MS ridge-lines. The input metallicities in the Geneva models are limited to $Z = 0.002$, 0.006 , and 0.014 (Z_\odot). The physical parameters adopted for our fits are included in Table 3 (rows 1–4). Our fits were based on initial estimates taken from previous publications. The typical age of NGC 330 is 20 Myr or $\log(t \text{ yr}^{-1}) = 7.30$ (McLaughlin & van der Marel 2005). For NGC 1805 and NGC 1818, the relevant numbers are 25 Myr to 40 Myr, i.e., $\log(t \text{ yr}^{-1}) = 7.40$ – 7.60 (Johnson et al. 2001), and for NGC 2164 it is 80 Myr, $\log(t \text{ yr}^{-1}) = 7.91$ (Mucciarelli et al. 2006). The best-fitting metallicities are $[\text{Fe}/\text{H}] = -0.82$ dex ($0.15Z_\odot$; McLaughlin & van der Marel 2005), -0.3 dex ($0.5Z_\odot$; Li et al. 2013a), 0.0 dex (Z_\odot ; Li et al. 2013a), and -0.4 – 0.0 dex ($0.4Z_\odot$ to Z_\odot ; Sagar & Richtler 1991) for NGC 330, NGC 1805, NGC 1818, and NGC 2164, respectively. The extinction, $E(B - V)$, for these clusters varies from 0.08 mag to 0.12 mag (Bessell 1991; Li et al. 2013a; Vallenari et al. 1991). The canonical distance moduli to the LMC and SMC are $(m - M)_0 = 18.49$ mag and 18.96 mag, respectively (de Grijs et al. 2014; de Grijs & Bono 2015).

Table 3. Physical parameters for the isochrones or synthetic clusters in Figs 3 and 4 (rows 1–4), Fig. 5 (rows 5–8), and Figs 6–9 (rows 9–12).

Cluster	$\log(t \text{ yr}^{-1})$	Z	$E(B - V)$ (mag)	$(m - M)_0$ (mag)	ω
NGC 330	7.30	0.002	N/A	19.00	0.00–0.95

Table 3 continued on next page

⁴ $\omega = 0.0, 0.1, 0.3, 0.5, 0.6, 0.7, 0.8, 0.9$ and 0.95

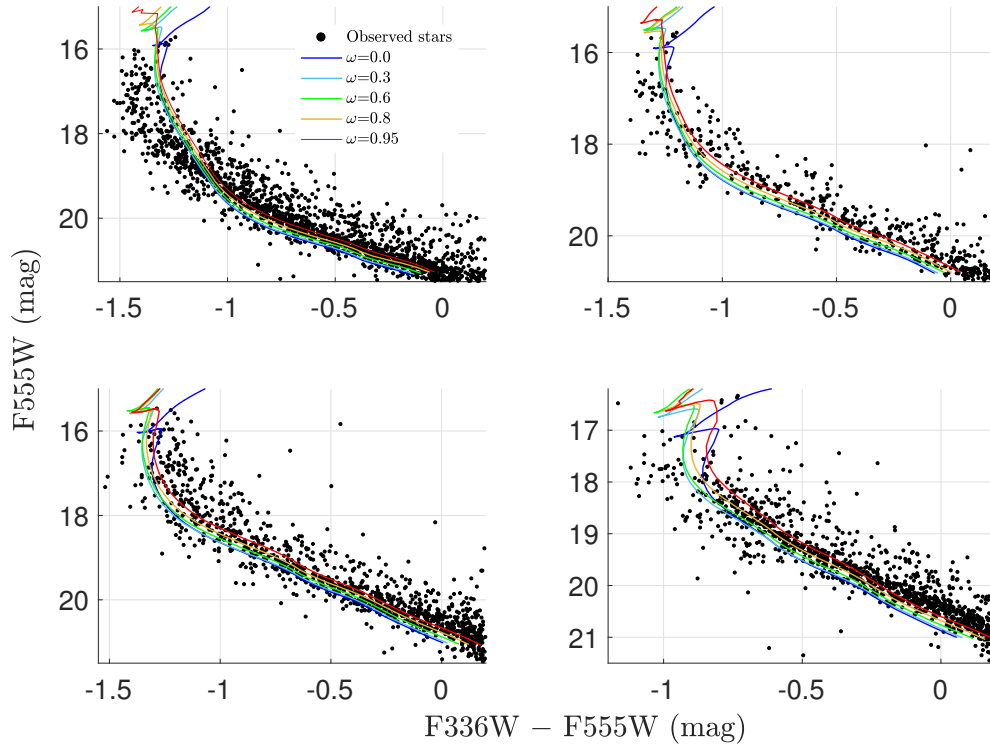


Figure 3. Observed CMDs and best-fitting isochrones based on the Geneva SYCLIST code. The solid lines of different colors are isochrones characterized by different rotation rates, as indicated in the legend. For reasons of clarity, we only display five isochrones with different rotation rates.

Table 3 (*continued*)

Cluster	$\log(t \text{ yr}^{-1})$	Z	$E(B - V)$ (mag)	$(m - M)_0$ (mag)	ω
NGC 1805	7.50	0.006	N/A	18.50	0.00–0.95
NGC 1818	7.55	0.014	N/A	18.55	0.00–0.95
NGC 2164	8.00	0.014	N/A	18.55	0.00–0.95
NGC 330	6.00,7.40,7.60	0.003	0.10	18.90	0.40
NGC 1805	6.00,7.30,7.60	0.006	0.12	18.40	0.40
NGC 1818	6.00,7.25,7.55	0.011	0.08	18.60	0.40
NGC 2164	7.70,7.85,8.00	0.011	0.10	18.55	0.40
NGC 330	6.00–7.60	0.002	N/A	19.00	0.00–0.95
NGC 1805	6.00–7.60	0.006	N/A	18.50	0.00–0.95
NGC 1818	6.00–7.55	0.014	N/A	18.55	0.00–0.95
NGC 2164	7.70–8.00	0.014	N/A	18.55	0.00–0.95

We show our fits in Fig. 3. We find that for three young star clusters (NGC 330, NGC 1805 and NGC 1818), the non- and fast-rotating isochrones converge in the MSTO region. Although isochrones with different rotation rates create a broadened region near the MSTO region of NGC 2164, the broadening still seems too narrow to fully explain its extended MSTO region. For all our clusters, the observed MS widths gradually increase toward the MSTO region. Our fits seem to show minor disagreements between the models and the observations.

Isochrone fitting alone cannot precisely describe the similarities between the models and the observations. In order to better demonstrate the reliability of our fits, for each cluster we constructed a synthetic CMD for comparison.

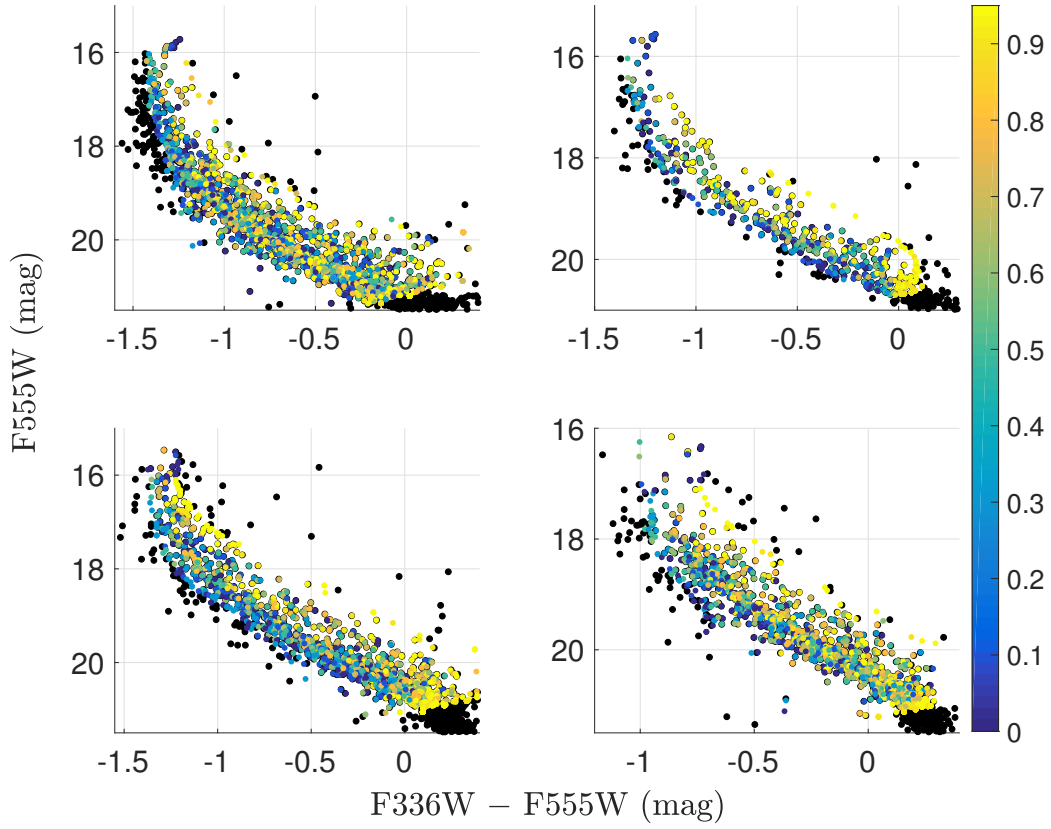


Figure 4. Synthetic CMDs for NGC 330, NGC 1805, NGC 1818, and NGC 2164. The color bar indicates the rotation rates of the simulated stars. For each cluster, we adopted 50% unresolved MS–MS binaries. The observed stars are indicated by black dots.

Our synthetic CMDs are based on the adopted isochrones, to which we added the same photometric uncertainties as pertaining to the real data. We used the method of [Milone et al. \(2012\)](#). We determined MS–MS binary fractions of $53.8 \pm 4.9\%$, $46.1 \pm 3.5\%$, $39.9 \pm 2.9\%$, and $53.3 \pm 4.5\%$ for NGC 330, NGC 1805, NGC 1818, and NGC 2164, respectively⁵. The average binary fraction of these four clusters is $\sim 48.3\%$. We thus include 50% of unresolved MS–MS binaries in each simulated CMD. If the mass of the secondary component of a simulated binary system below $1.7M_{\odot}$ (corresponding to the low-mass limit of the grid of B-type stars with different rotation rates in the Geneva models), we interpolate the magnitudes of the secondary star using the isochrones calculated based on the large grid ($M = 0.8\text{--}500M_{\odot}$, only two rotation rates; [Ekström et al. 2012](#); [Georgy et al. 2013](#)). Where necessary, we extrapolate outside the grid’s boundaries down to $0.08 M_{\odot}$ (i.e., the stellar hydrogen-burning limit).

For each CMD, we generated more than 3×10^6 artificial stars. Because the Geneva models can only generate rapidly rotating isochrones for stellar masses down to $1.7M_{\odot}$. The numbers of the corresponding stars in the CMDs of NGC 330, NGC 1805, NGC 1818, and NGC 2164 are 1827, 493, 1206, and 1234, respectively. The number of artificial stars is thus at least 1600 times larger than the numbers of stars in the observations. For each observed star, we selected the 10 nearest artificial stars from the synthetic CMD. Finally, we randomly selected one of these 10 fake stars as representative of the observed star. Using this procedure, if a simple stellar population (SSP) characterized by different stellar rotation rates and a realistic fraction of unresolved binaries could fully cover and match the observed MS region, the synthetic CMD should be almost identical to the observed CMD. We present our results in Fig. 4.

Fig. 4 shows that the use of only a coeval stellar population characterized by different stellar rotation rates cannot fully reproduce the observed wide MSs. There is an excess of blue MS stars who cannot be reproduced by our simulations. Our method shows that many simulated stars are non-rotating stars (i.e., $\omega = 0.0$). This is not surprising, because most fast-rotating stars would appear redder than their non-rotating counterparts. Since a fraction of the

⁵ These are the binary fractions for all mass ratios, under the assumption that the mass-ratio distribution is flat.

observed MS stars is too blue to be reproduced by our SSP models, our method is forced to select numerous non-rotating stars to try to cover those blue MS stars in the CMD. This confirms our speculation based on Fig. 3: all sample clusters exhibit populations of very blue stars that cannot be explained by a coeval stellar population, not even when adopting a range in stellar rotation rates. Because the synthetic CMDs have the same distributions of the photometric uncertainties as the observations, and the resulting synthetic CMDs are based on large samples, each containing more than 3×10^6 artificial stars, these additional blue MS stars thus cannot be explained by large scatter in the measurements. As shown in Fig. 2, only few background stars could contaminate the bright part of the MS; residual background contamination thus cannot explain these blue MS stars either. The additional blue stars may suggest the presence of young stellar populations.

We subsequently explored the age-spread scenario. We used the MIST models to describe the observations. The MIST models cover a large grid of single-star stellar evolution models, extending across all evolutionary phases for different stellar masses and metallicities (Paxton et al. 2011, 2013, 2015; Dotter 2016; Choi et al. 2016). The MIST 1.0 version includes a default rotational rate of $V/V_{\text{crit}} = 0.4 (\omega \sim 0.6)$ in the output isochrones. Huang et al. (2010) studied the rotational velocities of ~ 530 B-type stars. They found that the highest probability density occurs around $V/V_{\text{crit}} = 0.49$, which is close to the MIST default value. Using the Geneva models, we confirmed that the color difference between isochrones of $V/V_{\text{crit}} = 0.4$ and 0.49 is small (less than 0.02 mag in $U - V$ color). Given that the broadened sections of our clusters' MSs are expected to be mainly populated by B-type stars, an average rotational rate of $V/V_{\text{crit}} = 0.4 (\omega \sim 0.6)$ is thus a good approximation.

In Fig. 5 we show the outcome of our fits including age spreads. For each cluster, we have overplotted a young, a median, and an old isochrone onto the observations. The best-fitting young and old isochrones were determined by visual inspection, by comparing their loci to the blue and red edges of the MSs. The median isochrones were determined arbitrarily; they will be used to indicate the trends of the TO regions for different ages. The metallicities, extinction values, and distance moduli for these differently aged isochrones are the same: see Table 3 (rows 5–8).

As shown in Fig. 5, as regards our fits to the colors, the age-spread scenario works better than the stellar rotation scenario. We found that in order to fit the additional blue MS stars, the age range of the stellar population needs to extend to almost zero for NGC 330, NGC 1805, and NGC 1818. We simply adopted an age of 1 Myr to represent the zero-age population in our fits (but see below). For the relatively old cluster NGC 2164, an isochrone with age down to 50 Myr is required to fit the blue MS boundary. Our fits indicate that the age spreads in NGC 330, NGC 1805, NGC 1818, and NGC 2164 are 40 Myr, 40 Myr, 35 Myr, and 50 Myr, respectively.

However, the age spread model is not perfect either. The MIST models suggest that if the age spread were to reflect an extended star-formation history, a 1 Myr-old stellar population should contain a fraction of massive O-type and pre-MS stars. However, there is no obvious evidence of the presence of such objects. In NGC 330, a small number of stars are detected around the pre-MS locus, but we confirmed that they are background residuals, based on inspection of their spatial distribution. The absence of massive O-type and pre-MS stars indicates that the origin of such young stellar populations must be reconsidered. We will return to this issue in Section 4.

Based on their exploration of the TO region in the cluster NGC 1850, Correnti et al. (2017) suggested that the best solution may be a combination of stellar rotation and an age spread. We similarly explored the promise of the combination of an age spread and stellar rotation. The input parameters are presented in Table 3 (rows 9–12). The method we used is similar to that used for Fig. 4. This time, we generated artificial stars that are both different in age and rotation properties. For each observed star, we randomly selected an artificial star from among the 10 nearest candidates as its best representation. Our simulation was based on the Geneva database, because the Geneva models provide isochrones for different stellar rotation rates. Each time when we generated an SSP for a different stellar rotation rate, we compared its CMD with the observational counterpart, similarly to our analysis of Fig. 4. Again, we confirmed that even if we vary the isochronal age, the reproduction is not satisfactory. Specifically, once we adopted a young isochronal age for the synthetic CMD, a fraction of red MS stars could not be reproduced. This is a similar conclusion as that reached by Milone et al. (2016, their Fig. 10). Synthetic CMDs of stellar populations with different ages and rotation rates are presented in the right-hand panels of Figs 6–9. For a more direct comparison, we also included the observed CMDs (gray dots). In the synthetic CMDs, colors represent the ages of the simulated stars.

We first examined NGC 330. We found that if we use a combined model including an age spread and a distribution of stellar rotation rates, only a small number of blue MS stars would be poorly reproduced. We find that for the low-mass end of the main sequence, the contributions from young and old populations are not very different. However, for the MSTO region, the contributions from the young and old populations are indeed very different. Almost all young stars reproduce the observed stars located in the blue part of the MSTO region, while the old stars mainly contribute to the red part of the MSTO. This result further supports the notion that in order to reproduce the bluest

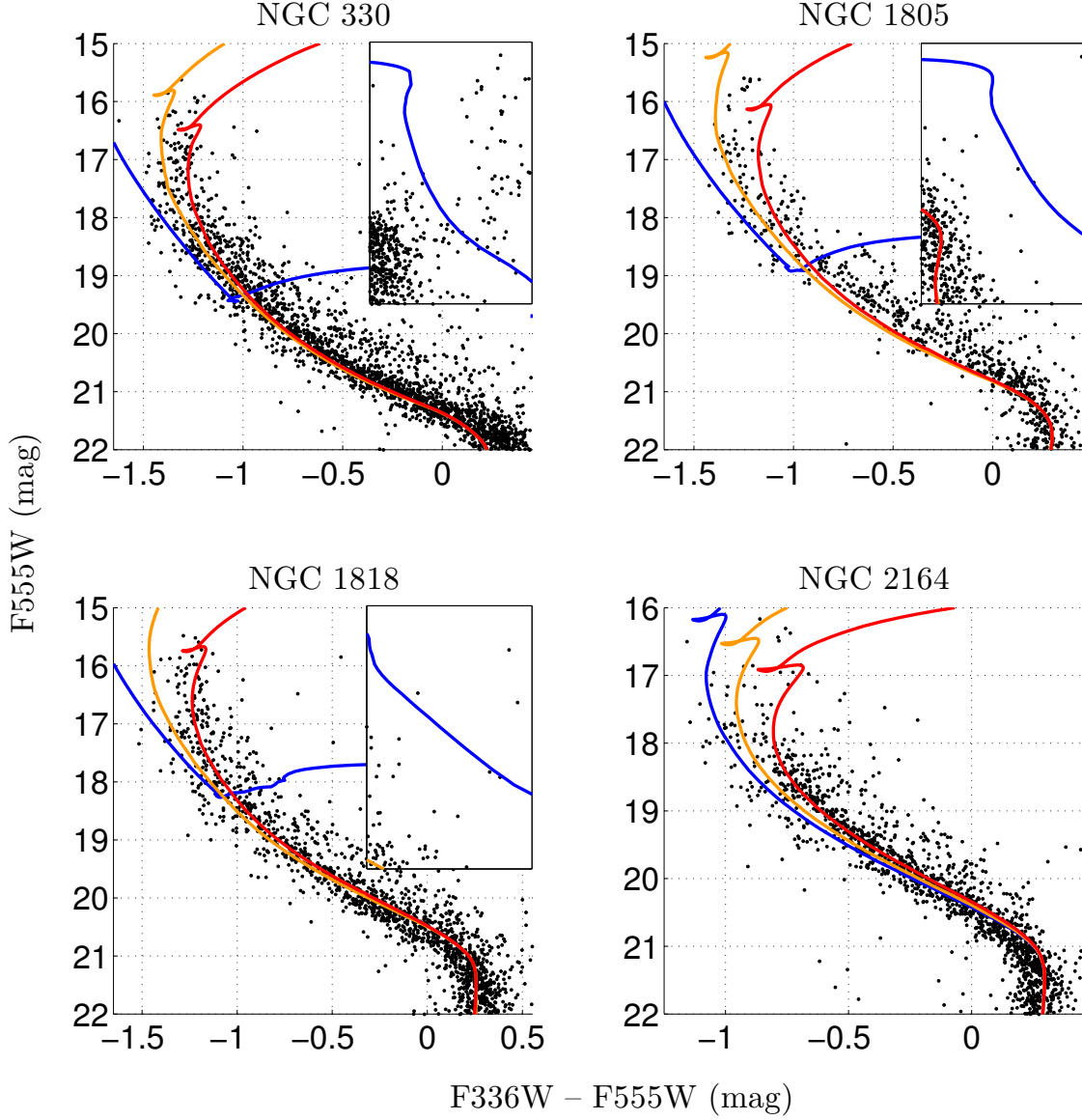


Figure 5. CMDs of the clusters NGC 330, NGC 1805, NGC 1818, and NGC 2164. The blue, orange, and red isochrones represent the loci of young, intermediate-age, and old stellar populations. For NGC 330, NGC 1805, and NGC 1818, subpanel are included to show the pre-MS region down to the bottom of the MS.

MS stars, a fraction of young stars is required.

The same result for NGC 1805 is shown in Fig. 7. The synthetic CMD of multiply-aged stellar populations is almost identical to the observations. Only three MS stars around $F555W \sim 18$ mag are not well reproduced. This is not surprising, because the synthetic CMD fully covers the region of the observed MS; for each observed star we should be able to find a corresponding artificial star with similar color and magnitude. This result stands in sharp contrast to the synthetic CMD of a coeval stellar population (see Fig. 4), where numerous additional blue MS stars in the range $16 \leq F555W \leq 19$ mag are not well reproduced.

This result also holds for NGC 1818, as shown in the right-hand panel of Fig. 8: almost all blue MS stars that appear in Fig. 4 are reproduced. Finally we show the same result for NGC 2164 in Fig. 9. Again, the simulated MS is significantly broadened compared with that of a single-aged stellar population. In summary, the cluster CMDs can be reproduced well by a combination of SSPs that cover an age range of 35–50 Myr and a wide variety of rotation rates.

At face value, the successful reproduction of the observations through a combination of an age range and a dispersion in rotation rates seems to indicate the need for an extended star-formation history for the clusters. However, the

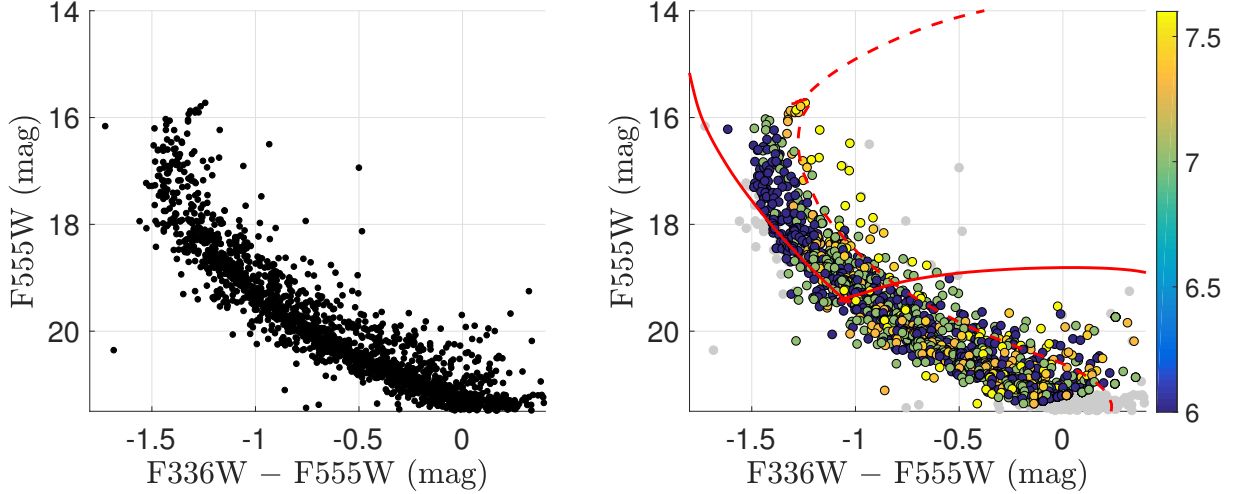


Figure 6. (Left) Observed CMD of NGC 330. (Right) Simulated CMD with various ages and rotational rates, and observed CMD (grey dots) of NGC 330. The color bar represents the ages of the simulated stars in the right-hand panel.

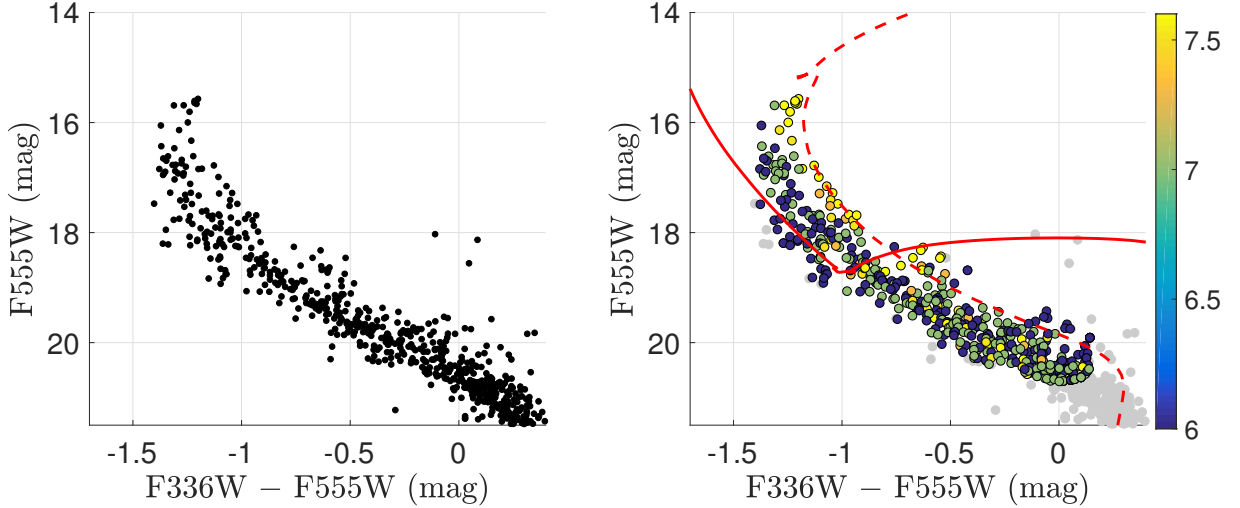


Figure 7. As Fig. 6, but for NGC 1805.

adoption of using a ‘nearest’ star to represent an observed star is complicated. This treatment is similar to the application of a mass truncation to the young stellar population, which thus avoids the appearance of massive O-type stars. This is indeed a contrived approach.

As we already emphasized, the origin of any ongoing star formation in these clusters is suspicious. In Figs 6–9, we also included the young isochrones adopted in Fig. 5, as well as the equal-mass binary locus of the corresponding old isochrone. Although these two lines seem to adequately describe the boundaries of the MSs, the young isochrone clearly predicts the presence of bright O-type and pre-MS stars. An absence of O-type stars would indicate an unphysical mass function, while the lack of pre-MS stars reflects the notion that star formation has long been terminated.

4. DISCUSSION

4.1. *Stellar Rotation?*

We will next discuss the possible physical interpretations of our observations. As deduced from our analysis of Figs 3 and 4, the observed wide MSTO regions cannot be fully explained by a coeval stellar population characterized by different stellar rotation rates. This is so, because the color separation between the non-rotating and fast-rotating MS stars is caused by gravity darkening (von Zeipel 1924), which would cause a fast rotator to have a lower surface temperature than its non-rotating counterpart. Using the Geneva models, we found that the reduction in surface

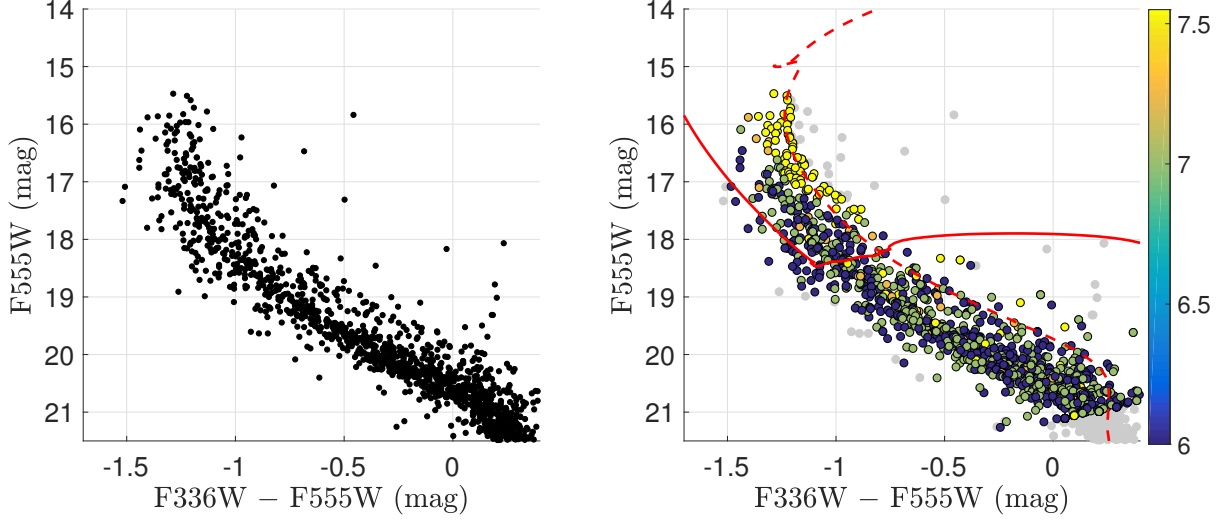


Figure 8. As Fig. 6, but for NGC 1818.

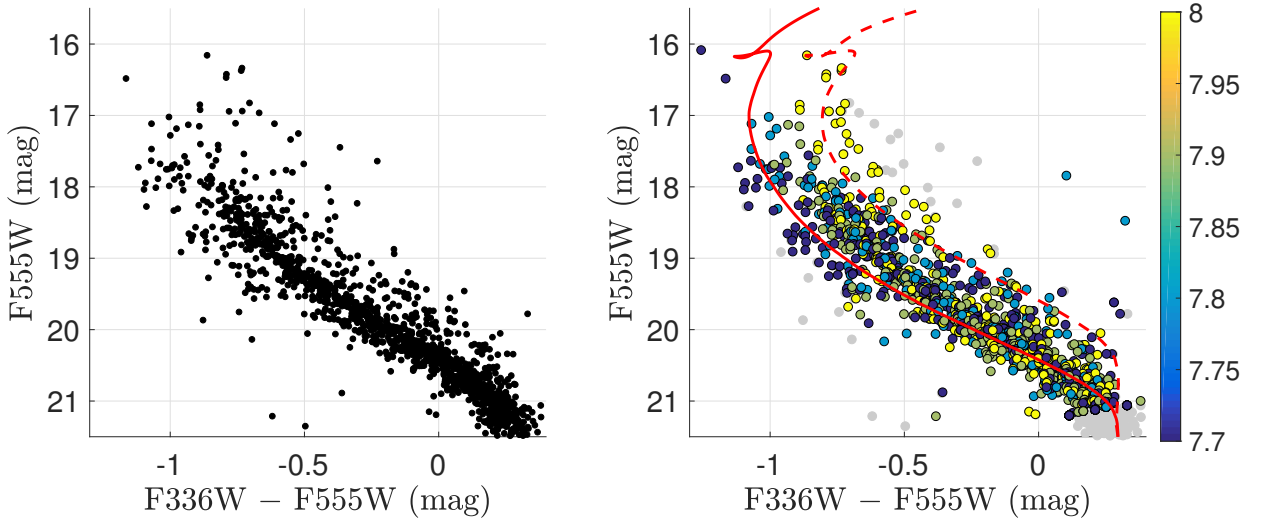


Figure 9. As Fig. 6, but for NGC 2164.

temperature caused by a rotation rate of $\omega = 0.95$ is roughly constant at 500–1000 K for all MS stars irrespective of their mass. This temperature difference is sufficient to produce a detectable color spread for late-B- or F-type stars. However, such a temperature difference only negligibly affects the colors of more massive, hot stars. In this paper, most stars located on the bright section of the MS have typical surface temperatures of $\sim 15,000$ – $20,000$ K. The color difference, $\Delta(F336W - F555W)$, owing to a reduction of ~ 500 – 1000 K in surface temperature is less than 0.1 mag for these stars.

The non-rotating and fast-rotating isochrones converge in the MSTO region, as illustrated by [Girardi et al. \(2011\)](#). This is because stellar rotation causes expansion of the stellar convective shell, leading to transportation of shell material to the stellar core. As a result, a rapidly rotating star will have a longer lifetime during the MS stage. This process is called rotational mixing. Rotational mixing renders the MSTO of a fast-rotating population brighter and bluer than that of a non-rotating population. This effect could therefore mask the reddening caused by the gravity darkening.

Because our sample clusters are so young, the observed wide MSs are mainly composed of early-B-type stars. The surface temperatures of these massive MS stars is too high for their colors to be significantly affected by gravity darkening. Rotational mixing causes populations characterized by different rotation rates to converge into a narrow

sequence at the TO region. All these factors conspire that stellar rotation cannot fully explain the observed broad MSTOs.

4.2. Extended Star Formation?

As we showed in Figs 6 to 9, to reproduce the observed broad MSTOs, an age spread of 35 Myr (NGC 1818) to 50 Myr (NGC 2164) is required. An age spread of ~ 10 Myr ($\Delta \log(t \text{ yr}^{-1}) \sim 0.1\text{--}0.2$ for the typical ages of NGC 330, NGC 1805, and NGC 1818; roughly equal to the timescale of initial gas expulsion) is insufficient. As Figs 6 to 9 clearly illustrate, only a stellar population with an age as young as 1 Myr could reach the positions of the bluest MS stars. Our result is in agreement with the conclusions of Milone et al. (2017) and Correnti et al. (2017).

Does this imply that all of our sample clusters have extended star-formation histories? One should be cautious as regards such speculations. We emphasize once again that the absence of O-type and pre-MS stars contradicts the ongoing star-formation hypothesis. It seems that the most massive stars in the blue stellar population are not more massive than those of the bulk stellar population. As we showed in Section 3, to reproduce the observed MSs, we have to assume a mass truncation for the young stellar population. This seems a contrived approach to reproduce the observations, which cannot be naturally explained by a invoking a scenario of extended star formation.

A possible explanation is that a few million-year-old stars may still be embedded in their natal dust cocoons, which would prevent us from observing them in the UV band. However, this cannot explain the presence of the very blue MS stars. Why would the very bright O-type stars be obscured while the B-type stars (and thus those blue MS stars) are discernible in the UV band? In addition, Bastian & Strader (2014) studied the gas and dust contents in NGC 330, NGC 1818, and NGC 2164; no significant gas residuals nor any dust were detected in these clusters. All these arguments thus challenge the continuous star-formation hypothesis.

We can estimate the minimum masses for our clusters to retain their gas using the equation from Georgiev et al. (2009),

$$M_{\text{cl}} \approx 100 v_{\text{esc}}^2 r_{\text{h}}, \quad (1)$$

where M_{cl} is the total mass of the cluster expressed in units of M_{\odot} , v_{esc} is the escape velocity of the initial gas in km s^{-1} , and r_{h} is the cluster's half-mass radius in pc. We assumed that the clusters' half-mass radii are equal to their half-light radii, r_{hl} ⁶. If star formation in these clusters can last for several tens of millions of years, numerous Type II supernova explosions should have taken place. The escaping gas can be accelerated to several hundred km s^{-1} . The corresponding minimum masses required to retain the initial gas in our sample clusters are $\log(M_{\text{cl}}/M_{\odot}) = 6.84, 6.46, 6.70$, and 6.64 (assuming a minimum escape velocity of 100 km s^{-1}). However, the current masses of NGC 330, NGC 1805, NGC 1818, and NGC 2164 are only $\log(M_{\text{cl}}/M_{\odot}) = 4.61, 3.70, 4.41$, and 4.18 , respectively (McLaughlin & van der Marel 2005). Clearly, it is difficult for these clusters to sustain long star-formation episodes by accreting their initial gas.

Another explanation to explain the occurrence of an extended star-formation episode that seems viable is that after the initial gas expulsion phase (~ 10 Myr), these clusters may still have been sufficiently massive to accrete the subsequent stellar ejecta of the asymptotic giant-branch (AGB) stars. The minimum velocity for the AGB stellar ejecta is about $v_{\text{esc}} = 10 \text{ km s}^{-1}$ (Renzini 2008; Li et al. 2016b). The minimum masses to retain the gas of the AGB ejecta for these clusters are $\log(M/M_{\odot}) = 4.84, 4.46, 4.70$, and 4.64 , which is still 1.7 (NGC 330) to 5.8 (NGC 1805) times the current cluster masses. Although the clusters would have lost their stellar mass through dynamical evaporation, this would not dramatically affect our clusters, because the typical timescale for such mass loss is expressed in units of billions of years (McLaughlin & Fall 2008; Li et al. 2016b).

In summary, although the observed broad MSs in our clusters indicate the possible presence of an age spread, it seems that such age spreads unlikely originate from extended star-formation histories.

4.3. Blue Straggler Stars?

An alternative explanation is that the population of puzzling blue MS stars are blue straggler stars (BSSs). Because BSSs are produced through binary mass transfer, mergers, or stellar collisions, their maximum mass does not exceed twice the mass of TO stars. This may explain the absence of O-type and pre-MS stars.

D'Antona et al. (2015) studied the split MS in the cluster NGC 1856. They speculated that all observed blue MS-component stars may hide a binary component. They suggested that the periods pertaining to these binary systems range from 4 to 500 days. Based on Kepler's Third Law, the relationship between the binary period, P , and its

⁶ We also adopted an average value of 0.1 for the coefficient f_c based on table 2 of Georgiev et al. (2009).

semi-major axis, a , is

$$P = 2\pi\sqrt{\frac{a^3}{G(M+m)}} = 2\pi\sqrt{\frac{a^3}{GM(1+q)}}, \quad (2)$$

where G is the usual gravitational constant, M and m are the masses of the primary and secondary stars, and $q = m/M$ is their mass ratio. Based on equation 3, we can calculate a in terms of P , M , and q :

$$a = \sqrt[3]{\frac{P^2 GM(1+q)}{4\pi^2}}. \quad (3)$$

Assuming that q ranges from 0 to 1, P from 4 to 500 days, and that the typical mass of the young-population stars in our clusters is $2M_\odot \leq M \leq 9M_\odot$, the resulting distribution of the semi-major axes ranges from $a = 0.06$ to 3.23 au. Using a Monte Carlo approach, we derived that the average length of the semi-major axis of the binary population is $a = 1.63$ au, with 23% of the binaries having semi-major axes $a \leq 1$ au (we adopted flat distributions for q , P , and M). This indicates the presence of a significant fraction of compact binaries, which may form a potential population for mass-transfer BSS candidates. This was also suggested by Yang et al. (2011). Specifically, the latter authors suggested that the eMSTO regions in intermediate-age star clusters include significant contributions from binary interactions and mergers.

However, the fraction of BSSs with respect to the bulk stellar population is usually very small (e.g., for the old LMC GCs, see Li et al. 2013b; Mackey et al. 2006). It is unclear how a cluster environment could produce such a large number of BSSs. To our knowledge, there are no direct observations of BSSs in YMCs. Xin et al. (2007) studied a large sample of (> 1 Gyr-old) Galactic open clusters. They found that the specific frequency of BSSs (i.e., the ratio of the number of BSSs to that of stars spanning a 2 mag range below the MSTO) ranges from 1% to 20%. Numerical simulations also show that the specific frequency of BSSs should be small during the early stages of a cluster's evolution (e.g., at an age of 50 Myr, the number of BSSs is fewer than 50 for a cluster that initially contains 100,000 stars; Lu et al. 2011; Hyski & Giersz 2013).

Despite this challenge, if the observed young stars are indeed BSSs, most should have been formed through binary mass transfer. Future studies should focus on their carbon and oxygen abundances to test this suggestion (Ferraro et al. 2006).

5. CONCLUSIONS

In this paper, we have studied the CMDs of the clusters NGC 330, NGC 1805, NGC 1818, and NGC 2164. They all exhibit broad MSs, which cannot be explained by a SSP with unresolved binaries and photometric uncertainties. We suggest that it is likely that most YMCs may exhibit wide MSs in their ultraviolet–visual CMDs.

We found that the gravity darkening caused by stellar rotation plays a very limited role in hot, massive, early-type MS stars. In the meantime, rotational mixing would cause an isochrone to have a TO position that is almost indistinguishable from that of a non-rotating isochrone. Therefore, a dispersion of stellar rotation velocities in coeval ensembles of stars cannot reproduce the observed wide MSs.

The failure of the stellar rotation scenario to fully reproduce the observations indicates that the age-spread scenario may still be viable. An age spread of 35–50 Myr is required to explain the observations. We confirm that a combination of an age spread and stellar rotation can adequately reproduce the observations for all sample clusters. Similar conclusion were derived previously for the ~ 100 –200-Myr old clusters NGC 1850 and NGC 1866 (Milone et al. 2017; Correnti et al. 2017). However, we argue that the apparent age spread is unlikely owing to continuous star formation. Indeed, the clusters' masses seem too small to sustain extended star-formation episodes. Moreover, the absence of O-type and pre-MS stars also contradicts the extended star-formation hypothesis.

We suggest that the young stars may be BSSs, which reduces the need for very massive O-type and pre-MS stars. However, if this were correct, it is not clear why the number of BSSs in the clusters should be comparable to the number of the bulk stellar population. To understand the origin of these young stars, details about their chemical composition and rotation rates are required.

We thank Choi Jieun (Harvard–Smithsonian Center for Astrophysics) for providing us with the relevant model database. C. L. is supported by the Macquarie Research Fellowship Scheme. R. d. G. and L. D. acknowledge research support from the National Natural Science Foundation of China through grants U1631102, 11373010, and 11633005. A. P. M. acknowledges support from the Australian Research Council through a Discovery Early Career Researcher

Award, number DE150101816.

REFERENCES

- Bastian, N., & de Mink, S. E. 2009, *MNRAS*, 398, L11
- Bastian, N., & Strader, J. 2014, *MNRAS*, 443, 3594
- Bastian, N., & Niederhofer, F. 2015, *MNRAS*, 448, 1863
- Bastian, N., Niederhofer, F., Kozhurina-Platais, V., et al. 2016, *MNRAS*, 460, L20
- Bertelli, G., Nasi, E., Girardi, L., et al. 2003, *AJ*, 125, 770
- Bessell, M. S. 1991, in: *The Magellanic Clouds*, Proc. IAU Symp. 148, Haynes, R., & Milne, D., eds, Dordrecht: Kluwer, p. 273
- Brandt, T. D., & Huang, C. X. 2015, *ApJ*, 807, 24
- Castelli, F., & Kurucz, R. L. 2004, in: *Modelling of Stellar Atmospheres*, Proc. IAU Symp. 210, Poster A20, Piskunov, N., Weiss, W. W., & Gray, D. F., eds, San Francisco: ASP; arXiv:astro-ph/0405087
- Choi, J., Dotter, A., Conroy, C., et al. 2016, *ApJ*, 823, 102
- Correnti, M., Goudfrooij, P., Bellini, A., Kalirai, J. S., & Puzia, T. H. 2017, *MNRAS*, 467, 3628
- D’Antona, F., Di Criscienzo, M., Decressin, T., et al. 2015, *MNRAS*, 453, 2637
- de Grijs, R., Wicker, J. E., & Bono, G. 2014, *AJ*, 147, 122
- de Grijs, R., & Bono, G. 2015, *AJ*, 149, 179
- de Grijs, R. 2017, *Nat. Astron.*, 1, 0011
- de Mink, S. E., Langer, N., Izzard, R. G., Sana, H., & de Koter, A. 2013, *ApJ*, 764, 166
- Dolphin A., DOLPHOT/WFC3 user’s guide, version 2.0. Available from <http://americano.dolphinsim.com/dolphin/dolphotWFC3.pdf>
- Dolphin A., DOLPHOT/WFPC2 user’s guide, version 2.0. Available from <http://americano.dolphinsim.com/dolphot/dolphotWFPC2.pdf>
- Dolphin A., DOLPHOT user’s guide, version 2.0. Available from <http://americano.dolphinsim.com/dolphot/dolphot.pdf>
- Dotter, A. 2016, *ApJS*, 222, 8
- Ekström, S., Georgy, C., Eggenberger, P., et al. 2012, *A&A*, 537, A146
- Ferraro, F. R., Sabbi, E., Gratton, R., et al. 2006, *ApJL*, 647, L53
- Georgiev, I. Y., Hilker, M., Puzia, T. H., Goudfrooij, P., & Baumgardt, H. 2009, *MNRAS*, 396, 1075
- Georgy, C., Ekström, S., Granada, A., et al. 2013, *A&A*, 553, A24
- Georgy, C., Granada, A., Ekström, S., et al. 2014, *A&A*, 566, A21
- Girardi, L., Rubele, S., & Kerber, L. 2009, *MNRAS*, 394, L74
- Girardi, L., Eggenberger, P., & Miglio, A. 2011, *MNRAS*, 412, L103
- Girardi, L., Goudfrooij, P., Kalirai, J. S., et al. 2013, *MNRAS*, 431, 3501
- Girardi, L. 2016, *ARA & A*, 54, 95
- Goudfrooij, P., Puzia, T. H., Kozhurina-Platais, V., & Chandar, R. 2011, *ApJ*, 737, 3
- Goudfrooij, P., Girardi, L., Kozhurina-Platais, V., et al. 2014, *ApJ*, 797, 35
- Gratton, R., Sneden, C., & Carretta, E. 2004, *ARA & A*, 42, 385
- Huang, W., Gies, D. R., & McSwain, M. V. 2010, *ApJ*, 722, 605
- Hypki, A., & Giersz, M. 2013, *MNRAS*, 429, 1221
- Johnson, R. A., Beaulieu, S. F., Gilmore, G. F., et al. 2001, *MNRAS*, 324, 367
- King, I. R. 1966, *AJ*, 71, 64
- Krause, M. G. H., Charbonnel, C., Bastian, N., & Diehl, R. 2016, *A&A*, 587, A53
- Li, C., de Grijs, R., & Deng, L. 2013a, *MNRAS*, 436, 1497
- Li, C., de Grijs, R., Deng, L., & Liu, X. 2013b, *ApJL*, 770, L7
- Li, C., de Grijs, R., & Deng, L. 2014a, *ApJ*, 784, 157
- Li, C., de Grijs, R., & Deng, L. 2014b, *Nature*, 516, 367
- Li, C., de Grijs, R., Bastian, N., et al. 2016a, *MNRAS*, 461, 3212
- Li, C., de Grijs, R., & Deng, L. 2016b, *RAA*, 16, 179
- Li, C., de Grijs, R., Deng, L., & Milone, A. P. 2017, *ApJ*, 834, 156
- Lu, P., Deng, L.-C., & Zhang, X.-B. 2011, *RAA*, 11, 1336
- Lupton, R. H., Fall, S. M., Freeman, K. C., & Elson, R. A. W. 1989, *ApJ*, 347, 201
- Mackey, A. D., Payne, M. J., & Gilmore, G. F. 2006, *MNRAS*, 369, 921
- Mackey, A. D., & Broby Nielsen, P. 2007, *MNRAS*, 379, 151
- McLaughlin, D. E., & van der Marel, R. P. 2005, *ApJS*, 161, 304
- McLaughlin, D. E., & Fall, S. M. 2008, *ApJ*, 679, 1272-1287
- Milone, A. P., Bedin, L. R., Piotto, G., & Anderson, J. 2009, *A&A*, 497, 755
- Milone, A. P., Piotto, G., Bedin, L. R., et al. 2012, *A&A*, 540, A16
- Milone, A. P., Bedin, L. R., Piotto, G., et al. 2015, *MNRAS*, 450, 3750
- Milone, A. P., Marino, A. F., D’Antona, F., et al. 2016, *MNRAS*, 458, 4368
- Milone, A. P., Marino, A. F., D’Antona, F., et al. 2017, *MNRAS*, 465, 4363
- Mucciarelli, A., Origlia, L., Ferraro, F. R., Maraston, C., & Testa, V. 2006, *ApJ*, 646, 939
- Niederhofer, F., Bastian, N., Kozhurina-Platais, V., et al. 2017, *MNRAS*, 465, 4159
- Piotto, G., Milone, A. P., Bedin, L. R., et al. 2015, *AJ*, 149, 91
- Paxton, B., Bildsten, L., Dotter, A., et al. 2011, *ApJS*, 192, 3
- Paxton, B., Cantiello, M., Arras, P., et al. 2013, *ApJS*, 208, 4
- Paxton, B., Marchant, P., Schwab, J., et al. 2015, *ApJS*, 220, 15
- Renzini, A. 2008, *MNRAS*, 391, 354
- Sagar, R., & Richtler, T. 1991, *A&A*, 250, 324
- Salinas, R., Pajkos, M. A., Strader, J., Vivas, A. K., & Contreras Ramos, R. 2016, *ApJL*, 832, L14
- Sarna, M. J., & De Greve, J.-P. 1996, *QJRAS*, 37, 11
- Scowcroft, V., Freedman, W. L., Madore, B. F., et al. 2016, *ApJ*, 816, 49
- Vallenari, A., Chiosi, C., Bertelli, G., Meylan, G., & Ortolani, S. 1991, *A&AS*, 87, 517
- von Zeipel, H. 1924, *MNRAS*, 84, 665
- Wilson, C. P. 1975, *AJ*, 80, 175
- Wu, X., Li, C., de Grijs, R., & Deng, L. 2016, *ApJL*, 826, L14
- Xin, Y., Deng, L., & Han, Z. W. 2007, *ApJ*, 660, 319
- Yang, W., Meng, X., Bi, S., et al. 2011, *ApJL*, 731, L37
- Yang, W., Bi, S., Meng, X., & Liu, Z. 2013, *ApJ*, 776, 112